

# Neutral Pions and $\eta$ Mesons as Probes of the Expanding Hadronic Fireball in Nucleus–Nucleus Collisions at SIS <sup>\*</sup>

Ralf Auerbeck

*Gesellschaft für Schwerionenforschung, Planckstr. 1, D-64291 Darmstadt, Germany*

---

## Abstract

The production of  $\pi^0$  and  $\eta$  mesons in collisions of light, intermediate–mass, and heavy nuclei at beam energies between 0.8A GeV and 2.0A GeV is discussed in the framework of a model assuming equilibrium at hadrochemical and thermal freeze–out, respectively. From the relative particle yields temperatures  $T_C$  of 56 – 90 MeV and baryon chemical potentials  $\mu_B$  of 780 – 675 MeV are deduced at chemical freeze–out. Midrapidity spectra of  $\pi^0$  and  $\eta$  mesons are consistent with the obtained temperatures if, in addition, the measured transverse expansion of the collision zone is taken into account. In contrast to results from similar analyses of AGS and SPS data the deduced freeze–out parameters are far below the phase boundary between a hadron gas and a quark–gluon plasma.

---

## 1 Introduction

During the last two decades the investigation of the properties of hadronic matter at high density and high temperature has become one of the key issues of nuclear physics. Relativistic nucleus–nucleus collisions offer the unique possibility to study nuclear matter under such extreme conditions. At incident energies around 1A GeV the formation of a hot and dense reaction zone, the so–called nuclear fireball, has been verified experimentally [1]. According to model calculations, nuclear matter can be compressed for time spans of  $\approx 10 - 15$  fm/c to densities of  $\approx 2 - 3$  times the nuclear groundstate density [2,3,4,5]. Simultaneously, temperatures up to  $\approx 100$  MeV may be reached and

---

<sup>\*</sup> Presented at the IV. TAPS Workshop, Mont Sainte Odile, France, September 1997

a substantial fraction of the nucleons participating in the collision is excited to heavier, short-lived resonance states which decay predominantly by meson emission [6,7,8]. Hence, the fireball at SIS-energies represents a system of interacting nucleons, resonances, and mesons. Under these conditions the onset of the partial restoration of chiral symmetry, which is a fundamental symmetry of quantum chromodynamics, could manifest itself in modifications of hadron properties inside the fireball. At beam energies of  $\approx 10A$  GeV, as they are available at the AGS accelerator facility at BNL (Brookhaven), even higher baryon densities and temperatures are reached in the initial stage of the fireball [9]. In addition to the chiral phase transition one may approach in those collisions already the phase transition from a hadron gas to a quark-gluon plasma due to the deconfinement of quarks and gluons. In such a scenario the fireball would no longer be purely hadronic during the whole collision process but the initial stage should be a partonic phase until hadronization takes place. At the SPS accelerator facility at CERN (Geneva), where the highest energy nuclear collisions can be studied using  $158A$  GeV Pb beams, the possibility exists that the phase boundary to quark matter has been crossed already, although evidence for the phase transition is still rather tentative [10].

It is the common goal of numerous experiments at SIS, AGS, and SPS to investigate the hadronic or partonic fireball, respectively. Since each relativistic nucleus-nucleus collision, irrespective of the initial beam energy, develops a hadronic phase in its final stage, the importance of studying the purely hadronic fireball as it is formed in the SIS-energy regime is evident. Various observables, e.g. particle yields, spectra, and correlations are sensitive to different parameters of the fireball. Only the combination of all observables may finally give a complete picture of  $A$  GeV heavy-ion collisions which up to now are not fully understood.

In this paper we concentrate on  $\pi^0$  and  $\eta$ -meson production as probes of the fireball. Chapter 2 summarizes briefly some basic features of the time evolution of relativistic nucleus-nucleus collisions as far as meson production is concerned. On the basis of the presently available systematics of  $\pi^0$  and  $\eta$ -meson production the motivation for a thermal-model ansatz to describe hadronic matter at freeze-out is given. In the chapters 3 and 4 the model of a hadron gas in thermal and hadrochemical equilibrium is described in detail and applied to the fireball as observed at SIS. After fixing the model parameters by experimental data, the part of the nuclear-matter phase diagram probed by hadronic observables at SIS is determined and compared to corresponding results from AGS and SPS. Furthermore, the chemical composition of the fireball at freeze-out is estimated and the consistency of particle yields and spectra is studied.

## 2 $\pi^0$ and $\eta$ Mesons from the Fireball at SIS

### 2.1 Nucleus–Nucleus Collisions at SIS

Numerous investigations of relativistic nucleus–nucleus reactions have shown that for central collisions at SIS the relative motion of target and projectile matter in the reaction zone almost comes to rest. While for heavy target–projectile combinations at moderate energies an isotropically expanding source at midrapidity has been observed [11], indications for incomplete stopping have been found in rapidity–density distributions for energies above  $\approx 1A$  GeV [12]. The size of the fireball thus arising depends on the centrality of the collision. Following the participant–spectator model, the geometrical overlap of the two nuclei determines the number of nucleons  $A_{part}$  which are directly involved. In addition the energy available in the nucleon–nucleon system  $\sqrt{s} - 2m_N$  can be obtained from the projectile energy, so that the initial conditions of the system are fixed. In the subsequent development the energy is transformed into the excitation of thermal and collective degrees of freedom: it turns into heat and provides the mass stored in the resonance states, and it builds up compression and produces the flow of the expanding matter.

In a simplified picture the mesons are trapped during the compression phase in a cyclic process of generation, absorption, and re–emission, exemplified for nucleons  $N$ ,  $\pi$  mesons, and  $\Delta$  resonances by  $NN \rightleftharpoons N\Delta \rightleftharpoons NN\pi$ . Within this approach the bulk of the mesons are released only with the onset of the expansion phase, when due to the decreasing matter density mesons and baryons decouple. This implies that hadronic probes reflect only the final state of nucleus–nucleus collisions and do not provide direct insight into the early, high–density phase of the collision as leptonic probes would do since they are not affected by the strong interaction. The moment in the expansion process when particles cease to interact strongly is called freeze–out. One distinguishes between chemical freeze–out and thermal freeze–out which correspond to those points in time when the relative abundances or the momentum distributions of the particles, respectively, are no longer changed. Obviously only inelastic collisions of nucleons, resonances, and mesons can change the relative particle yields while the momentum distributions are governed by the total interaction cross sections of these particles in the fireball. Therefore, chemical freeze–out does not occur after thermal freeze–out. Even in this simplified sudden freeze–out scenario one has to make sure that for the determination of freeze–out parameters only such observables are combined with each other which are fixed approximately simultaneously. In our ansatz particle yields reflect chemical freeze–out while momentum distributions reflect thermal freeze–out. The latter, however, are not purely thermal spectra in the sense that they follow Boltzmann distributions but they are modified by resonance decays

and reflect in addition collective flow phenomena.

It is an interesting question to what extent the fireball at freeze-out can be described in terms of thermal and hadrochemical equilibrium. Equilibrium could be achieved through frequent scattering of particles in the fireball and it would be reached without any doubt if only the lifetime of the fireball would be sufficiently long. It has been shown that at AGS and SPS the hadronic observables including strange particles are in quite good agreement with such a scenario [13,14,15,16], while at SIS the situation is still unclear. Only recently it has been reported that midrapidity momentum spectra of nonstrange particles measured in central  $^{58}\text{Ni} + ^{58}\text{Ni}$  collisions are consistent with thermal equilibrium in the energy regime from 1A GeV to 2A GeV if in addition collective radial flow is taken into account [12]. For the same reactions also agreement with chemical equilibrium has been claimed [17]. This analysis, however, was based on proton, deuteron, thermal charged pion, and  $\Delta(1232)$ -resonance yields. The latter were obtained by decomposing the pion momentum spectra into a thermal component and into a component from resonance decay. In this paper we follow a different strategy: in order to keep the possibility to distinguish chemical and thermal freeze-out as individual stages in the time evolution of relativistic nucleus-nucleus collisions we strictly confine ourselves to an isolated discussion of relative particle yields and momentum distributions, respectively, without combining these informations. In order to keep the thermal model as simple as possible we do not take into account particles with open strangeness since at SIS energies their production rate is very small. Furthermore, an additional model parameter, the strangeness chemical potential  $\mu_S$ , which, however, could be fixed by requesting strangeness conservation, would be necessary to incorporate strangeness consistently into the thermal model. With respect to strange particles, only recently Cleymans and co-workers have claimed that at 1.93A GeV the particle yields including the strange hadrons agree with a complete chemical equilibrium scenario at freeze-out [18]. This would mean that not only the nonstrange and strange hadrons among themselves could be equilibrated separately, but even equilibrium between both the strange and the nonstrange sectors would have been established.

## *2.2 Results from $\pi^0$ and $\eta$ meson production experiments*

The neutral  $\pi^0$  and  $\eta$  mesons which have large decay branches into pairs of photons represent unique probes for the expanding fireball and therefore provide the basis for our discussion. Pions and  $\eta$  mesons are the only mesons with substantial production rates at SIS energies. While the pionic degree of freedom is also covered by the spectroscopy of the charged members of the multiplet, it is only through gamma-ray spectroscopy that the  $\eta$  meson becomes observable

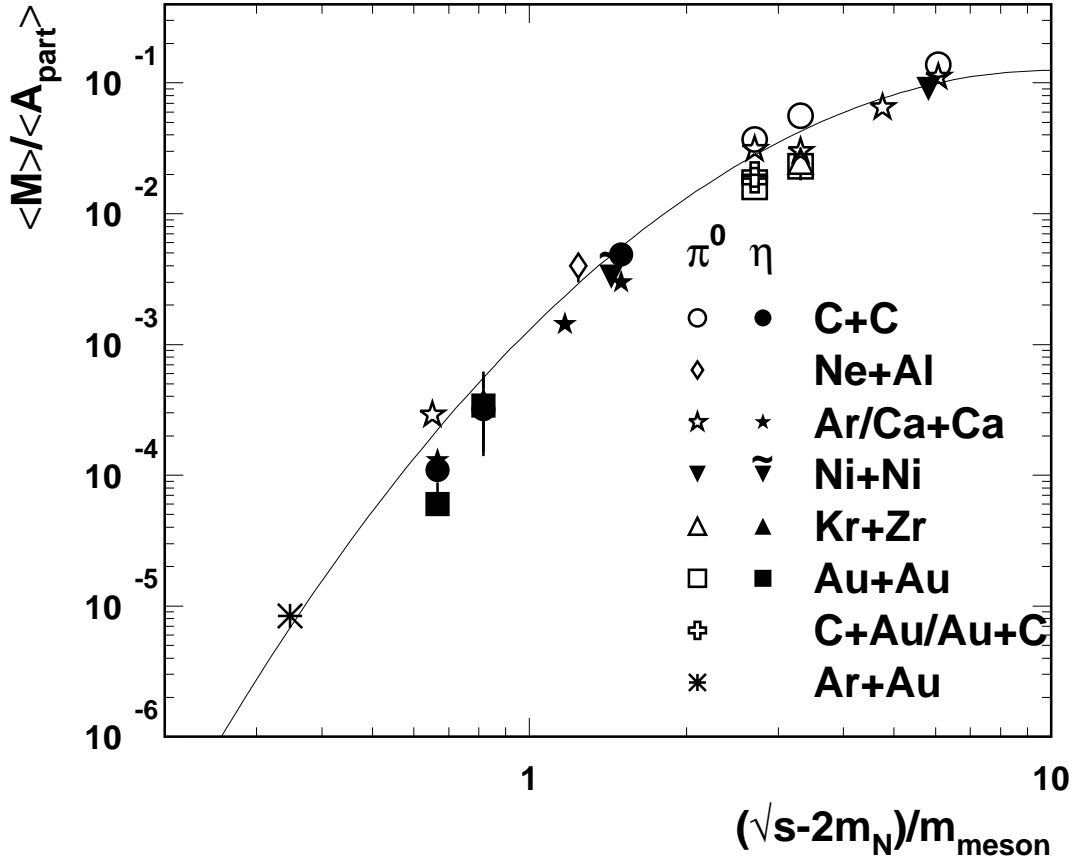


Fig. 1. Average  $\pi^0$  and  $\eta$ -meson multiplicities per average number of participants in nucleus-nucleus collisions as a function of the energy available in the nucleon-nucleon system. The data are taken from [19,20,21,22,23,24,25,26,27,28,29]. The line represents a fit, taking into account also charged-meson production in addition [7].

in nucleus-nucleus collisions. These two neutral mesons can be simultaneously identified by a two-photon invariant-mass analysis of coincident photon pairs. During the last almost ten years the TAPS collaboration performed a series of systematic meson-production experiments covering incident energies from  $0.1A$  GeV to  $2.0A$  GeV. These measurements have established an extended data base for  $\pi^0$  and  $\eta$  production in light ( $^{12}\text{C} + ^{12}\text{C}$ ), intermediate ( $^{40}\text{Ar}$ ,  $^{40}\text{Ca} + ^{\text{nat}}\text{Ca}$ ,  $^{58}\text{Ni} + ^{58}\text{Ni}$ ,  $^{86}\text{Kr} + ^{\text{nat}}\text{Zr}$ ) and heavy systems ( $^{197}\text{Au} + ^{197}\text{Au}$ ) [19,20,21,22,23,24,25,26,27,28,29]. The primary information are the spectral distributions of the mesons, measured down to zero transverse momentum in narrow bins around midrapidity, and the meson yields, which are determined in the same rapidity intervals and are then extrapolated to the full solid angle. All data concerning the experiments  $^{40}\text{Ar} + ^{\text{nat}}\text{Ca}$  at  $0.18A$  GeV [27],  $^{58}\text{Ni} + ^{58}\text{Ni}$  at  $1.9A$  GeV [24], and  $^{40}\text{Ca} + ^{\text{nat}}\text{Ca}$  at  $2.0A$  GeV [28] presented in this paper are not yet submitted for publication and should therefore be regarded as preliminary results.

The first important result is obtained from the systematic investigation of the

meson yields. Fig. 1 shows the average meson multiplicities  $\langle M \rangle$ , measured in inclusive reactions of various systems, normalized to the average number of participating nucleons  $\langle A_{part} \rangle$  as a function of the energy  $\sqrt{s} - 2m_N$  available in the  $NN$  system normalized to the corresponding meson mass. A steep rise of the relative yields with increasing energy is visible. In addition, a weaker dependence on the size of the collision system is observed with the clear tendency for smaller inclusive yields in the heavier systems. This has also been observed in charged-pion production experiments [30,31]. In first approximation all data points fall onto a smooth curve indicating that the meson-production probabilities mainly depend on the available energy. This is quite remarkable because  $\pi^0$  and  $\eta$  production proceed through different baryon resonances:  $\pi^0$  mesons mainly originate from  $\Delta(1232)$ -resonance decays, while the heavier  $\eta$  mesons essentially come from the  $N(1535)$  resonance which, at SIS energies, is the only significantly populated baryon resonance with a large decay channel into  $\eta$  mesons. The fact that the specific production mechanism seems not to influence the observed meson yields significantly may be interpreted as a first indication for meson emission from an equilibrated source.

The second important result concerns the average transverse momenta  $\langle p_t \rangle$ . Fig. 2 shows  $\langle p_t \rangle$  of  $\pi^0$  and  $\eta$  mesons as a function of the energy available in the  $NN$  system. Although the experimental uncertainties for the  $\eta$  data are large compared to the  $\pi^0$  data, the  $\eta$  transverse-momentum spectra reveal at a given energy a tendency towards larger mean values  $\langle p_t \rangle$  which is manifest around  $2.0A$  GeV beam energy. To give a measure for the expected order of magnitude of  $\langle p_t \rangle$ , it can be noted that for the decay of  $\Delta(1232)$  and  $N(1535)$  resonances at rest one would get  $\langle p_t \rangle_{\pi^0} = 225 \text{ MeV}^1$  and  $\langle p_t \rangle_{\eta} = 182 \text{ MeV}$ , respectively. For both mesons  $\langle p_t \rangle$  increases with the available energy which could be interpreted in terms of a considerable heating of the collision zone or a gradually growing population of the full resonance-mass distributions. For  $\pi^0$  mesons the rise of the average transverse momenta becomes smaller with increasing energy which is supported by a measurement of  $\langle p_t \rangle$  for  $\pi^-$  mesons produced at  $3.37A$  GeV bombarding energy [32]. The steep rise of the meson-production yields on the one hand and the onset of a saturation of average transverse momenta on the other hand clearly indicate that with increasing bombarding energy the fraction of available energy converted into massive particles becomes larger compared to the chaotic motion of particles in the fireball.

Finally, the distributions of the transverse mass  $m_t$  of  $\pi^0$  and  $\eta$  mesons are discussed. At midrapidity the transverse mass of a particle is equivalent to its total energy in the center-of-mass system. Following [33] the transverse-mass distribution of particles with mass  $m$ , emitted isotropically from a thermal

---

<sup>1</sup> Throughout this paper we follow the usual convention  $c = \hbar = 1$ .

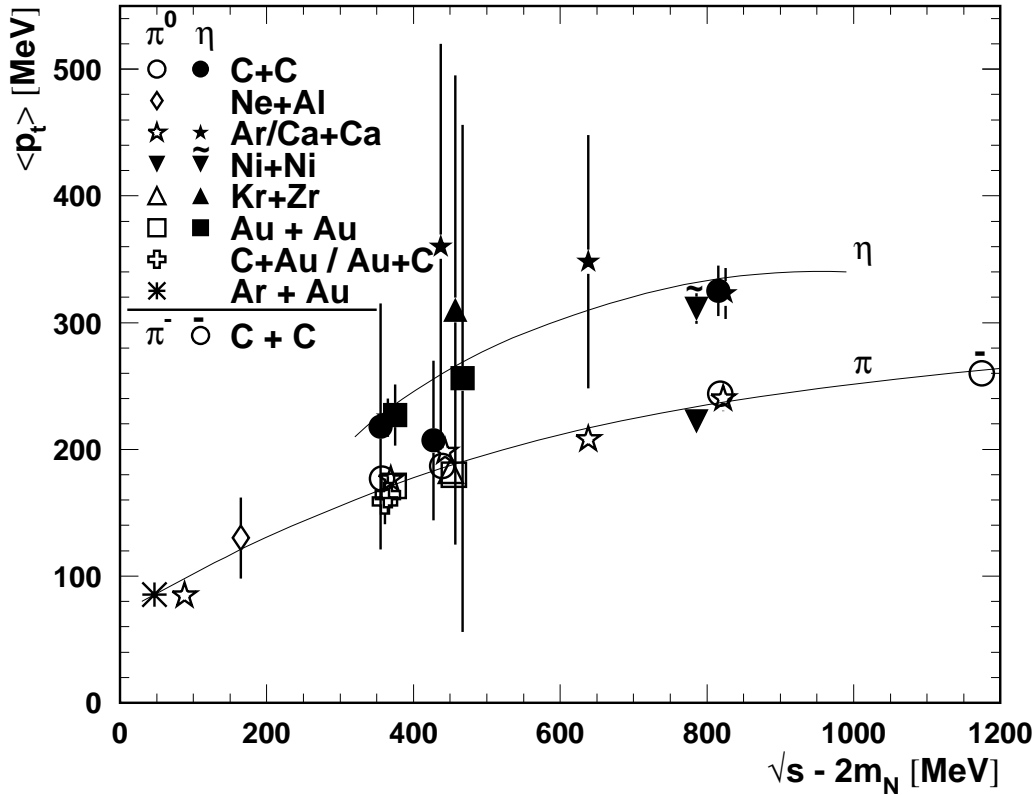


Fig. 2. Average  $\pi^0$  and  $\eta$ -meson transverse momenta measured in narrow rapidity intervals around midrapidity as a function of the energy available in the nucleon-nucleon system. The data are taken from the same experiments as listed in Fig. 1. The data points around available energies of 365 MeV (0.8A GeV beam energy) and 447 MeV (1.0A GeV beam energy) are shifted slightly on the energy axis with respect to their nominal position to resolve the error bars. Lines interpolating the  $\pi^0$  and  $\eta$  data, respectively, are drawn to guide the eyes. A  $\pi^-$  point taken from [32] has been added to the data set.

source and characterized by a Boltzmann temperature  $T_B$ , can approximately be described by

$$\frac{1}{m_t^2} \frac{d\sigma}{dm_t} \propto \exp\left(\frac{-m_t}{T_B}\right) \quad \text{with} \quad m_t = \sqrt{m^2 + p_t^2} \quad (1)$$

In Fig. 3 transverse-mass distributions of  $\pi^0$  and  $\eta$  mesons are plotted together with fits according to the parametrization given in Eq. 1 for three different collision systems at incident energies near 2A GeV. Within each reaction the  $\pi^0$  and  $\eta$  spectra exhibit almost identical inverse-slope parameters  $T_B$  which in addition do not change significantly with the mass of the colliding nuclei. Such a behaviour, the so-called  $m_t$  scaling, is well known in high-energy physics [34,35]. Having in mind the different production mechanisms for both meson species it is furthermore quite remarkable that for  $m_t \geq m_\eta$  the  $\pi^0$  and  $\eta$

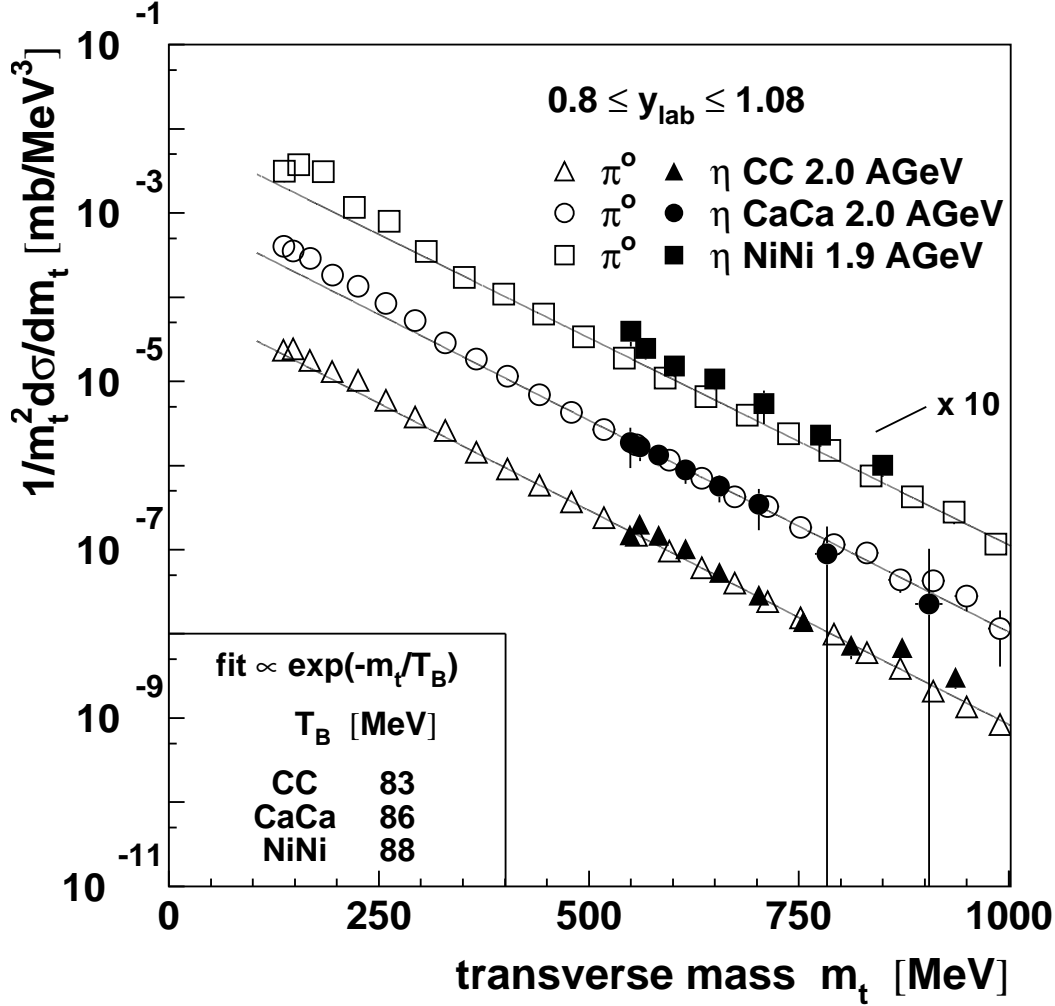


Fig. 3. Transverse-mass spectra of  $\pi^0$  and  $\eta$ -mesons as observed in the systems  $^{12}\text{C}+^{12}\text{C}$  [25] and  $^{40}\text{Ca}+^{nat}\text{Ca}$  [28] at 2.0A GeV beam energy and in  $^{58}\text{Ni}+^{58}\text{Ni}$  [24] at 1.9A GeV. The distributions are divided by the square of the transverse mass. In this representation midrapidity particle spectra from a source in thermal equilibrium are expected to exhibit a purely exponential spectrum. The solid lines represent exponential fits to the  $\pi^0$  data for  $m_t \geq 400$  MeV.

data roughly fall on one common line for all systems. This indicates that the energy required to produce a given transverse mass completely determines the relative abundance of the meson species near midrapidity. For low  $m_t$ , however, individual differences become apparent. Fig. 3 shows a systematic enhancement over the exponential rise extrapolated from the high- $m_t$  region if one goes from the light to the heavier systems. Possible mechanisms that have been suggested to account for this fact involve enhanced pion rescattering through resonance states in the heavier systems [36] and multiple pion decay of heavy resonances [37]. The same observation, namely the  $m_t$  scaling on an absolute scale and the low- $m_t$  enhancement in heavier systems, is not



only manifest at  $2A$  GeV but has been recognized at various energies down to  $0.8A$  GeV and seems to be a general feature of heavy-ion collisions in the SIS-energy regime [20,24,25,26,28,29]. Although  $m_t$  scaling does not prove that the meson source actually has reached thermal or hadrochemical equilibrium, the particle spectra of such an equilibrated source would be dominated by phase space as it is observed.

In summary, the systematic study of  $\pi^0$  and  $\eta$  meson yields and momentum distributions reveals strong indications for the hypothesis that these mesons may be emitted from a source in hadrochemical and thermal equilibrium.

### 3 Particle Yields and Chemical Freeze-Out in a Hadron-Gas Model

#### 3.1 Formalism of the Hadron-Gas Model

In our ansatz we assume that at the point of chemical freeze-out the fireball can be described in terms of an equilibrated hadron gas. As constituents of this ideal gas we take into account nucleons, deuterons, pions,  $\eta$  mesons, and all nonstrange baryon resonances up to a mass of 1.76 GeV, which corresponds to  $\sqrt{s} - m_N$  for the nucleon-nucleon system at  $2A$  GeV beam energy.

Nuclear matter in hadrochemical equilibrium has a particle composition characterized by a temperature  $T_C$  and a baryon chemical potential  $\mu_B$ . Considering the grand-canonical ensemble description of noninteracting fermions and bosons the particle-number densities  $\rho_i$  are given by integrals over the particle momentum  $p$ :

$$\rho_i = \frac{g_i}{2\pi^2} \int_0^\infty \frac{p^2 dp}{\exp[(E_i - \mu_B B_i)/T_C] \pm 1} \quad (2)$$

where  $g_i$  is the spin-isospin degeneracy,  $E_i$  the total energy in the local rest-frame, and  $B_i$  the baryon number of the particle species  $i$ . The  $\pm$  sign refers to the different statistics for fermions or bosons, respectively.

Eq. 2 can not be applied to the fireball at SIS directly but only after the inclusion of two modifications. To account for the fact that the fireball occupies only a finite volume, a surface correction has to be included. For an estimate of this correction we assume a spherical volume with radius  $R$  giving a momentum dependent correction factor  $f(pR)$  [38,39] which has to be multiplied

with the integrand in Eq. 2:

$$f(pR) = 1 - \frac{3\pi}{4pR} + \frac{1}{(pR)^2} \quad (3)$$

Introducing this correction leads to a decrease of individual particle–number densities down to 60 – 70 % of the uncorrected values for reasonable radius parameters. Particle yield ratios, however, are much less affected by the correction since there the correction almost cancels out. The radius parameter should be chosen such that the number of baryons inside the spherical volume is in reasonable agreement with the average number of nucleons participating in the collision. We use a constant radius parameter of 5.5 fm for all beam energies. If one assumes that chemical freeze–out may occur at baryon densities in the range between 0.2 and 0.6  $\rho_0$  (see below) the corresponding freeze–out volume would then contain  $\approx 23 - 70$  baryons. We verified that in our model analysis a variation of  $R$  by  $\pm 2$  fm changes the resulting temperatures and chemical potentials by less than 5 %.

The second modification is related to the fact that resonances do not have a fixed mass but exhibit a broad mass distribution. In contrast to thermal–model analyses of AGS and SPS data, a reasonable treatment of mass distributions can not be neglected in the 1A GeV energy regime since in this case the energy available in the  $NN$  system is small compared to the difference in mass between the nucleon and the resonances except for the  $\Delta(1232)$  resonance. That is the reason why the  $\Delta(1232)$  is by far the most abundantly populated resonance and why all the other resonances are populated predominantly in the tails of their mass distributions towards lower masses. Eq. 2 therefore has to be folded with normalized mass distributions  $A_i(m)$  which are  $\delta$  functions for all particle species except resonances. The following scheme to parametrize resonance mass distributions is to a large extent adopted from [37].

We distribute the resonance masses according to Lorentzian functions  $A_R(m)$  which are determined by the mean resonance masses  $m_R$  and the mass dependent total and partial decay widths  $\Gamma(m)$ :

$$A_R(m) = \frac{m^2 \Gamma_{tot}(m)}{(m^2 - m_R^2)^2 + m^2 \Gamma_{tot}^2(m)} \quad \text{with} \quad \Gamma_{tot} = \Gamma_{1\pi} + \Gamma_{2\pi} + \Gamma_{\eta} \quad (4)$$

We use the following parametrizations for the partial decay widths  $\Gamma(m)$  where the mean masses  $m_R$  and widths  $\Gamma_R$  at  $m_R$  are taken from [40]:

- For the pion decay width of the  $\Delta(1232)$  resonance we adopt the parametriza-

tion given by Koch et al. [41]

$$\Gamma(q) = \Gamma_R \frac{m_\Delta}{m} \left( \frac{q}{q_R} \right)^3 \left( \frac{q_R^2 + \delta^2}{q^2 + \delta^2} \right)^2 \quad (5)$$

where  $m$  is the actual mass of the  $\Delta(1232)$  resonance.  $q$  and  $q_R$  are the pion three momenta in the restframe of the resonance with mass  $m$  and  $m_\Delta$ , respectively. The parameter  $\delta$  in the cutoff function has the value  $\delta = 300$  MeV.

- The  $1\pi$  and  $\eta$  decay widths of the higher baryon resonances are given by

$$\Gamma(q) = \Gamma_R B_{1\pi,\eta} \left( \frac{q}{q_R} \right)^{2l+1} \left( \frac{q_R^2 + \delta^2}{q^2 + \delta^2} \right)^{l+1} \quad (6)$$

where  $B_{1\pi,\eta}$  is the branching ratio of the resonance into the  $1\pi$  or  $\eta$  decay channel at  $m_R$ , respectively,  $l$  is the angular momentum of the emitted meson, and  $q$  and  $q_R$  are the momenta of the meson in the restframe of the decaying resonance as defined above. In this case we use

$$\delta^2 = (m_R - M_N - m_{\pi,\eta})^2 + \frac{\Gamma_R^2}{4} \quad (7)$$

It has to be noted that the only resonance decaying into the  $\eta$  channel in our ansatz is the  $N(1535)$  resonance.

- The  $2\pi$  decay widths of higher baryon resonances are described in terms of one-step processes. This is in contrast to [37] where in a first step a higher baryon resonance decays into a  $\Delta(1232)$  or  $N(1440)$  resonance and a pion or into a nucleon and a  $\rho$  or  $\sigma$  meson, and where in a second step the intermediate resonance decays after propagation through the nuclear medium into a nucleon and a pion or into a nucleon and two pions. Since the population of higher resonances is small compared to the  $\Delta(1232)$  population we simplify this procedure by treating the  $2\pi$  decay as a direct process where the resonance decays into a nucleon and an object with angular momentum  $l = 0$  and twice the pion mass which subsequently decays into two pions. The partial decay widths can then be written in complete analogy to the  $1\pi$  and  $\eta$  decay width.
- Additional decay channels are neglected.

Furthermore, one could consider an excluded-volume correction to take into account the hadron-hadron hard-core repulsion or in other words the difference between a real and an ideal hadron gas. Since such a correction does not play a significant role for particle-yield ratios as demonstrated in [16] we stick to the ideal hadron-gas model. Another argument to omit the excluded volume correction is the fact that chemical freeze-out seems to occur at baryon densities of the order of half the nuclear groundstate density or even less as discussed below. The hadron gas therefore is rather dilute which justifies the assumption of non-interacting particles at chemical freeze-out.

Finally, the isospin asymmetry in collisions of heavy nuclei, which has to be considered if the model analysis for example relies on charged-pion yields, is not taken into account in the present analysis. This is adequate since our approach is based on the isospin-independent  $\eta$ -meson yields and the neutral-pion yields which in the isobar model correspond to one third of the total pion yields irrespective of the actual isospin asymmetry in the system.

In summary, the equation we finally use to evaluate the particle-number densities within our hadron-gas model reads as follows:

$$\rho_i = \frac{g_i}{2\pi^2} \int_0^\infty f(pR)p^2 dp \int_0^\infty \frac{A_i(m) dm}{\exp\left[\left(\sqrt{m^2 + p^2} - \mu_B B_i\right)/T_C\right] \pm 1} \quad (8)$$

Because we have parametrized the resonance-mass distributions using mass-dependent partial decay widths we can easily calculate the particle-number densities of mesons originating from any individual resonance decay, which turns out to be essential for the determination of the model parameters from experimental data. If  $\rho_{1\pi,2\pi,\eta}^{res}$  is defined as the particle-number density of pions or  $\eta$ -mesons stemming from a specific decay channel of an individual resonance one obtains

$$\rho_{1\pi,2\pi,\eta}^{res} = \frac{w g_i}{2\pi^2} \int_0^\infty f(pR)p^2 dp \int_0^\infty \frac{\Gamma_{1\pi,2\pi,\eta}(m) A_i(m) dm}{\Gamma_{tot}(m) \exp\left[\left(\sqrt{m^2 + p^2} - \mu_B B_i\right)/T_C\right] \pm 1} \quad (9)$$

with  $w = 1$  in the case of one-pion or  $\eta$ -meson decay and  $w = 2$  for the two-pion decay of a resonance.

### 3.2 Determination of the Model Parameters from Experimental Data

For a given beam energy the values of the two parameters of the hadron-gas model – the temperature  $T_C$  and the baryon chemical potential  $\mu_B$  – can be derived from at least two relative abundances of the constituents. The  $\pi^0$  and  $\eta$ -meson yields are particularly suited for such an analysis, as these particles unambiguously arise from the fireball. We base our analysis on the system-size averaged ratios  $\langle M_{\pi^0} \rangle / \langle A_{part} \rangle$  and  $\langle M_\eta \rangle / \langle M_{\pi^0} \rangle$  as compiled in Tab. 1 (see also Fig. 1). The measured ratios are related to the particle-number densities calculated within the model by two equations:

$$\left(\frac{\langle M_{\pi^0} \rangle}{\langle A_{part} \rangle}\right)_{exp} = \frac{\left(\rho_\pi + \sum_{Res} \rho_{1\pi}^{Res} + \rho_{2\pi}^{Res}\right)/3}{\rho_N + 2\rho_D + \sum_{Res} \rho_{Res}} (\mu_B, T_C) \quad (10)$$

Table 1

Mean inclusive  $\pi^0$  multiplicities  $\langle M_{\pi^0} \rangle$  relative to the average number of participating nucleons  $\langle A_{part} \rangle$  and mean inclusive  $\eta$ -meson multiplicities  $\langle M_{\eta} \rangle$  relative to  $\langle M_{\pi^0} \rangle$  measured for various target-projectile combinations in the beam-energy range from 0.8A GeV to 2.0A GeV. The system-size averaged values are given in addition. The 2.0A GeV Ca and 1.9A GeV Ni data are still preliminary. \*For the average the latter have been upscaled by  $\approx 10\%$  to 2.0A GeV using the fit of the energy dependence as shown in Fig. 1.

$E$ [A GeV]	System	$\frac{\langle M_{\pi^0} \rangle}{\langle A_{part} \rangle}$ [%]	$\frac{\langle M_{\eta} \rangle}{\langle M_{\pi^0} \rangle}$ [%]	Reference
0.8	$^{12}\text{C}+^{12}\text{C}$	$3.7 \pm 0.3$	$0.31 \pm 0.11$	[25]
0.8	$^{40}\text{Ar}+^{nat}\text{Ca}$	$3.1 \pm 0.5$	$0.41 \pm 0.04$	[26]
0.8	$^{197}\text{Au}+^{197}\text{Au}$	$1.6 \pm 0.3$	$0.38 \pm 0.10$	[29]
0.8	$^{12}\text{C} + ^{197}\text{Au}$	$1.8 \pm 0.2$	—	[25]
0.8	$^{197}\text{Au} + ^{12}\text{C}$	$2.0 \pm 0.2$	—	[25]
0.8	Average	$2.6 \pm 0.3$	$0.39 \pm 0.06$	
1.0	$^{12}\text{C}+^{12}\text{C}$	$5.6 \pm 0.4$	$0.57 \pm 0.14$	[25]
1.0	$^{40}\text{Ar}+^{nat}\text{Ca}$	$3.0 \pm 0.3$	$1.3 \pm 0.8$	[20,21]
1.0	$^{86}\text{Kr}+^{nat}\text{Zr}$	$2.5 \pm 0.7$	$1.3 \pm 0.5$	[20,21,22]
1.0	$^{197}\text{Au}+^{197}\text{Au}$	$2.3 \pm 0.5$	$1.4 \pm 0.5$	[20,21,22]
1.0	Average	$4.0 \pm 0.4$	$1.06 \pm 0.41$	
1.5	$^{40}\text{Ar}+^{nat}\text{Ca}$	$6.5 \pm 0.5$	$2.2 \pm 0.4$	[20,21]
2.0	$^{12}\text{C}+^{12}\text{C}$	$13.8 \pm 1.4$	$3.6 \pm 0.4$	[25]
2.0	$^{40}\text{Ca}+^{nat}\text{Ca}$	$11.1 \pm 1.1$	$2.7 \pm 0.3$	[28]
1.9	$^{58}\text{Ni}+^{58}\text{Ni}$	$8.6 \pm 0.9$	$3.3 \pm 0.4$	[24]
2.0	Average*	$11.3 \pm 1.1$	$3.34 \pm 0.37$	

$$\left( \frac{\langle M_{\eta} \rangle}{\langle M_{\pi^0} \rangle} \right)_{exp} = \frac{\rho_{\eta} + \rho_{\eta}^{N(1535)}}{\left( \rho_{\pi} + \sum_{Res} \rho_{1\pi}^{Res} + \rho_{2\pi}^{Res} \right) / 3} (\mu_B, T_C) \quad (11)$$

To deduce  $\mu_B$  and  $T_C$  we determine within our model the chemical potentials and temperatures for which the calculated ratios are in agreement with the experimental values for  $\langle M_{\pi^0} \rangle / \langle A_{part} \rangle$  and  $\langle M_{\eta} \rangle / \langle M_{\pi^0} \rangle$ , respectively. Each ratio therefore defines an area in the parameter plane  $T_C$  versus  $\mu_B$ . Fig. 4 shows the resulting areas for the four considered beam energies 0.8, 1.0, 1.5, and 2.0A GeV.. The ratio  $\langle M_{\pi^0} \rangle / \langle A_{part} \rangle$  is strongly correlated with  $\mu_B$ . To increase  $\langle M_{\pi^0} \rangle / \langle A_{part} \rangle$  smaller values for

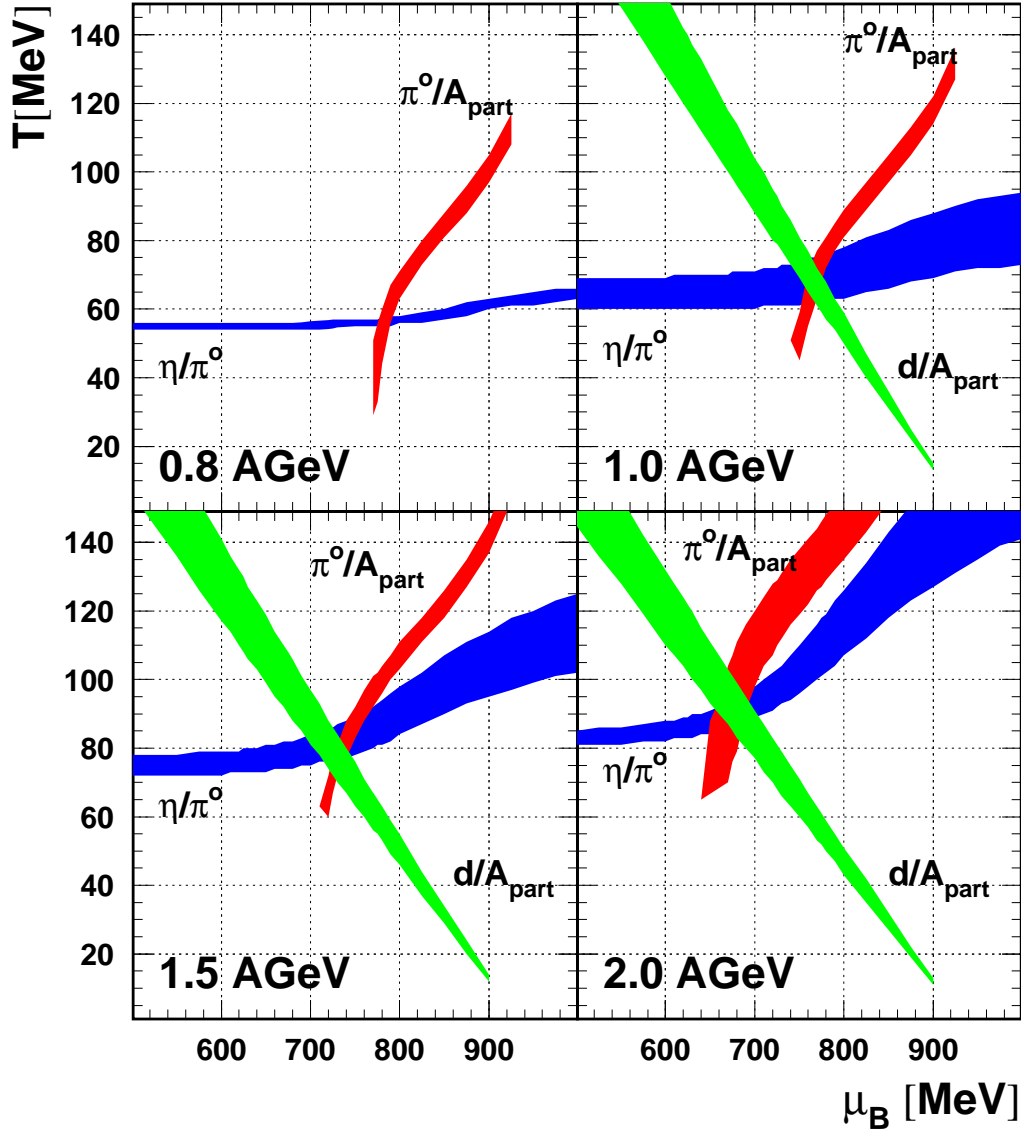


Fig. 4. Determination of chemical freeze-out parameters: for a given beam energy the two measured particle ratios  $\langle M_{\pi^0} \rangle / \langle A_{part} \rangle$  and  $\langle M_{\eta} \rangle / \langle M_{\pi^0} \rangle$  define two bands in the parameter plane  $(T_C, \mu_B)$  as described in the text. The four panels show these bands for beam energies of 0.8, 1.0, 1.5, and 2.0 A GeV. The freeze-out parameters are determined by the  $T_C$  and  $\mu_B$  values where the two bands cross each other. Except for the 0.8 A GeV case additional bands are shown which are defined by deuteron-to-nucleon ratios measured in central  $^{58}\text{Ni}+^{58}\text{Ni}$  collisions near the considered beam energies [12].

the chemical potential of the hadron gas are needed. In contrast to that, the ratio  $\langle M_{\eta} \rangle / \langle M_{\pi^0} \rangle$  is mainly correlated with  $T_C$ . With increasing  $\langle M_{\eta} \rangle / \langle M_{\pi^0} \rangle$  larger values for the hadron-gas temperature are necessary to obtain agreement between experimental and calculated ratios. For all beam energies the areas defined by the experimental boundary conditions

Table 2

Chemical freeze-out parameters  $T_C$  and  $\mu_B$  obtained from inclusive  $\pi^0$  and  $\eta$ -meson yields for the four considered beam energies.

$E$ [ $A$ GeV]	$T_C$ [MeV]	$\mu_B$ [MeV]
0.8	$56 \pm 2$	$780 \pm 10$
1.0	$70 \pm 5$	$770 \pm 15$
1.5	$83 \pm 7$	$745 \pm 20$
2.0	$90 \pm 6$	$675 \pm 20$

cross each other exactly once and therefore determine the temperature and the baryon chemical potential of the hadron gas at chemical freeze-out in an unambiguous way. In addition, bands corresponding to deuteron-to-nucleon ratios measured by the FOPI collaboration [12] in central  $^{58}\text{Ni} + ^{58}\text{Ni}$  collisions at beam energies of  $1.06A$  GeV,  $1.45A$  GeV, and  $1.93A$  GeV, respectively, are shown in Fig. 4. Obviously also these ratios are in nice agreement with the chemical freeze-out parameters obtained from inclusive  $\pi^0$  and  $\eta$ -meson yields. The results are summarized in Tab. 2. The analysis reveals a systematic increase of the freeze-out temperature from 56 to 90 MeV between 0.8 and  $2.0A$  GeV which is accompanied by a reduction of the baryon chemical potential from 780 to 675 MeV. The corresponding baryon density at chemical freeze-out is approximately 0.2 – 0.6 times the nuclear groundstate density which is in reasonable agreement with results from other analyses even at higher energies [14,15,17].

Fig. 5 shows our results within the phase diagram of hadronic matter together with other  $(T_C, \mu_B)$  values obtained from particle-production experiments at SIS, AGS, and SPS energies [14,15,17,42]. The data points are connected by a line to symbolize the chemical freeze-out curve of hadronic matter. In contrast to the AGS and SPS results the deduced chemical freeze-out parameters at SIS energies are far below the phase boundary between a hadron gas and a quark-gluon plasma. Results dealing with thermal freeze-out, which are also shown in Fig. 5, are discussed in the following chapter.

Having determined the chemical freeze-out parameters one can study the chemical composition of the hadronic fireball within the hadron-gas model. Fig. 6 shows the calculated relative populations of baryon species at chemical freeze-out as a function of the energy available in the nucleon-nucleon system together with the system-size averaged relative meson multiplicities  $\langle M_{\pi^0, \eta} \rangle / \langle A_{part} \rangle$  as given in Tab. 1. The hatched areas correspond to the relative populations of nucleons and deuterons (summed),  $\Delta(1232)$  and  $N(1535)$  resonances as the main sources of pions and  $\eta$  mesons, respectively, and the sum of all remaining  $\Delta$  and  $N$  resonances. With increasing available energy the fraction of baryons excited into resonance states at chemical freeze-out grows from  $\approx 2\%$  at  $0.8A$  GeV beam energy to  $\approx 15\%$  at  $2.0A$  GeV. The

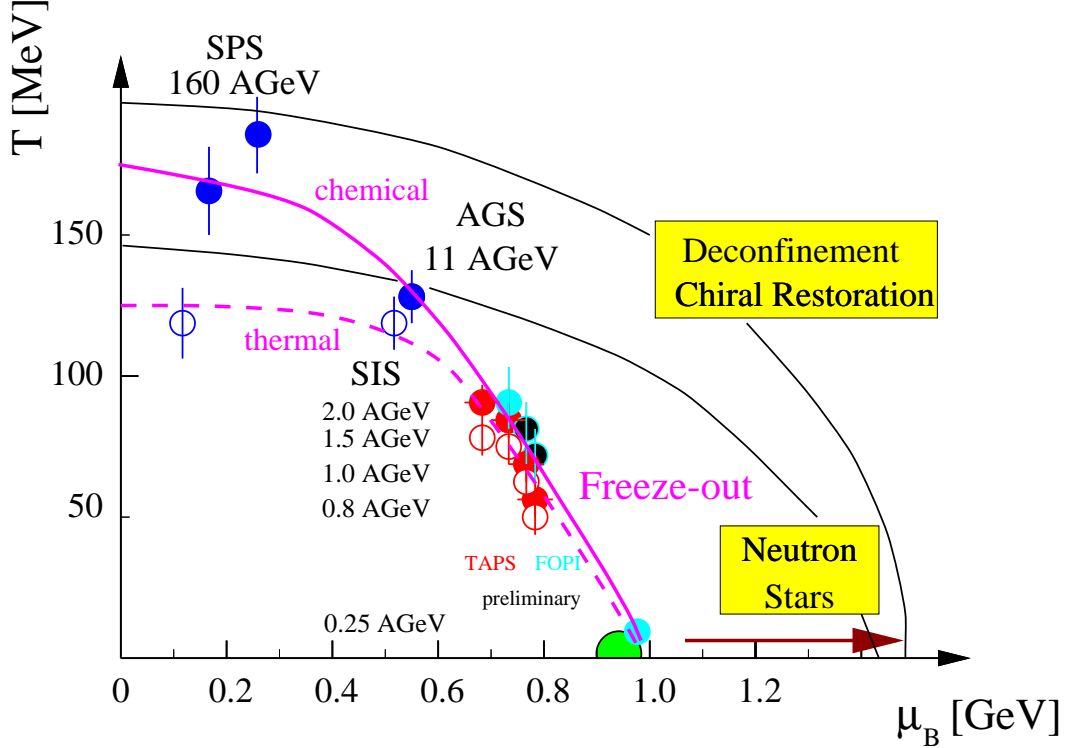


Fig. 5. Phase diagram of hadronic matter: the temperatures  $T$  and baryon chemical potentials  $\mu_B$  derived from yield ratios of particles produced in nucleus–nucleus collisions at different incident energies. Results of this work are plotted together with results taken from [14,15,17,42]. The solid curve through these data points represents the curve for chemical freeze–out of hadronic matter. Open data points represent parameter pairs for thermal freeze–out and are connected by a corresponding freeze–out curve (dashed).

$\Delta(1232)$  resonance is populated most abundantly since it is the lowest mass baryon resonance. The ratio of heavier resonances to the  $\Delta(1232)$  increases from  $\approx 5\%$  to  $\approx 15\%$  if one goes from low to high energies. Furthermore, it is obvious that the decay of resonances still excited at chemical freeze–out is not sufficient to account for the meson multiplicities observed asymptotically in the detector. Consequently, a sizeable fraction of resonance decays occurs before freeze–out is reached: at chemical freeze–out  $\approx 60\%$  of the pions and  $\approx 90\%$  of the  $\eta$  mesons are not bound in baryon resonances but are already present as free mesons.

Finally, one can extrapolate the resonance population at chemical freeze–out to the population in the high–density phase of the collision. Guided by microscopic model calculations [37,43] which quite consistently give a maximum baryon density of  $\rho_{max} \approx 2.5 \rho_0$  and which predict ratios around 0.6 for the number of  $\Delta(1232)$  resonances present at maximum compression relative to the number of asymptotically observed pions, one obtains an initial resonance density of  $0.6 \times 0.113 \times 3 \approx 0.2 \rho_{max} \approx 0.5 \rho_0$  at 2.4 GeV beam energy. Since in



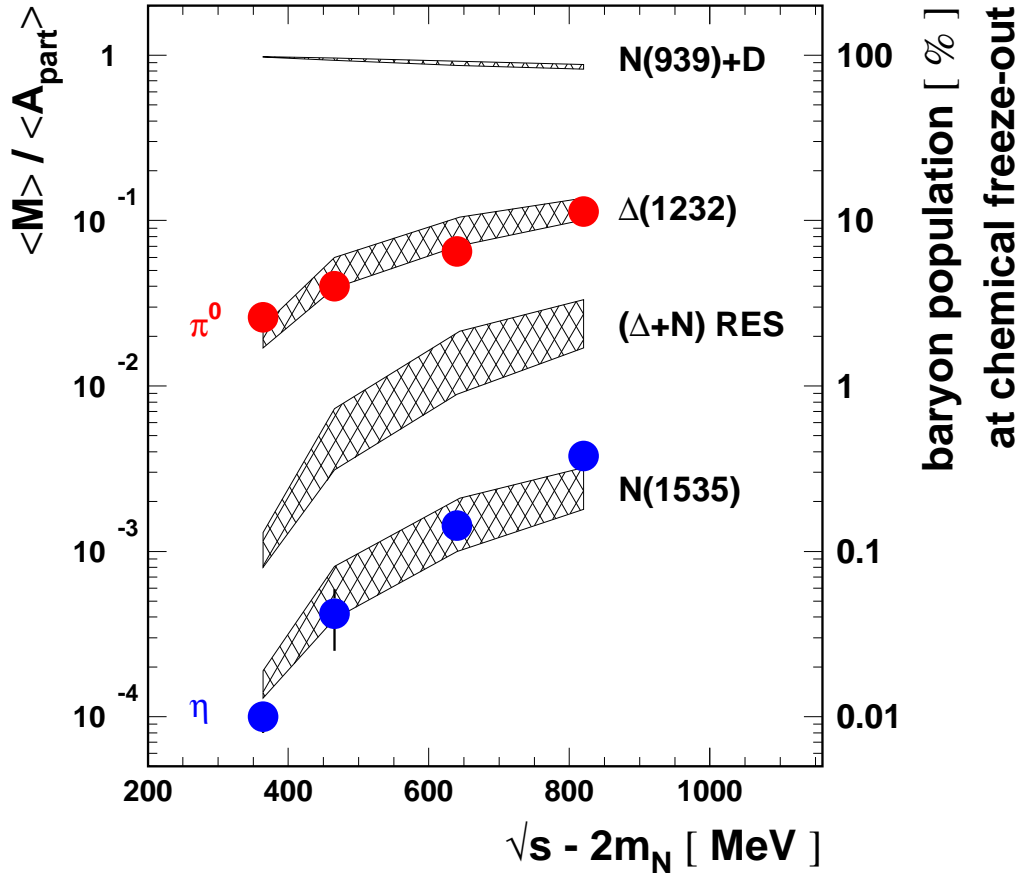


Fig. 6. Inclusive  $\pi^0$  and  $\eta$ -meson yields as function of the energy available in the nucleon–nucleon system (left scale). The data points represent system–size averaged values from various collision systems (see Tab. 1). In addition, the hatched bands show the relative populations of nucleons and deuterons (summed), the  $\Delta(1232)$  resonance, the  $N(1535)$  resonance, and the sum of all remaining  $\Delta$  and  $N$  resonances (right scale), as obtained from the hadron–gas model described in the text. Only one third of the  $\Delta(1232)$  resonances decays into neutral pions. Considering that due to the limited available energy the  $N(1535)$  resonance is predominantly populated at masses below the nominal mass of 1535 MeV it is comprehensible that less than 50 %, which is the branching ratio at the nominal mass, of these resonances decay into the  $\eta$  channel.

the high–density phase of the collision the baryon–resonance density becomes comparable to the nuclear groundstate density, hadronic matter in that stage is often referred to as resonance matter [6,8].

## 4 Particle Spectra and Thermal Freeze-Out in a Thermal Model

While particle yields contain information about chemical freeze-out parameters as discussed in the preceding chapter, particle spectra reflect the nucleus–nucleus collision process at the stage of thermal freeze-out in our simple sudden freeze-out scenario. Even if the system reaches global thermal equilibrium at freeze-out the spectra, however, do not follow pure Boltzmann distribution functions, but they are modified by resonance decays and they furthermore reflect collective flow phenomena.

We present here an analysis of the midrapidity  $\pi^0$  and  $\eta$ -meson spectra within the blast model proposed by Siemens and Rasmussen [44]. In this model, a fireball in thermal equilibrium expands isotropically. All particles in the fireball share a common temperature  $T$  and radial-flow velocity  $\beta_r$ , which are the two parameters that characterize the fireball at thermal freeze-out. The transverse-mass spectra are then described by

$$\frac{1}{m_t^2} \frac{d^2 N}{dm_t dy} \propto \cosh y \exp(-\gamma_r E/T) \left[ \left( \gamma_r + \frac{T}{E} \right) \frac{\sinh \alpha}{\alpha} - \frac{T}{E} \cosh \alpha \right] \quad (12)$$

where  $\gamma_r = 1/\sqrt{1 - \beta_r^2}$ ,  $\alpha = (\gamma_r \beta_r p)/T$ , and  $E$ ,  $p$ , and  $y$  are the total energy, momentum and rapidity of the considered particle in the center-of-mass system. The modification of the spectra compared to pure Boltzmann distributions becomes more significant the heavier the considered particle species is.

Since pions and  $\eta$  mesons have low masses their spectra are not very sensitive to the radial-flow velocity. Therefore a fit to the transverse-mass spectra using  $T$  and  $\beta_r$  both as free parameters allows to determine the freeze-out parameters only with very large uncertainties. To overcome this difficulty, we take  $\beta_r$  from the systematics of transverse-flow velocities for different collision systems and bombarding energies as published in [45]. Values for  $\beta_r$  between 0.25 and 0.35 are found to be a reasonable choice in the considered range of incident beam energies. To determine the thermal freeze-out parameter  $T$  we then fit the measured midrapidity transverse-mass spectra of  $\pi^0$  and  $\eta$  mesons using Eq. 12, where we vary only  $T$  and keep  $\beta_r$  constant. In the case of the pion spectra, we furthermore restrict the fit to  $m_t \geq 400$  MeV since the low  $m_t$  region is expected to be modified by resonance decays. As an example Fig. 7 shows the meson  $m_t$  spectra measured in the systems  $^{40}\text{Ar}/^{40}\text{Ca} + ^{nat}\text{Ca}$  together with two fits for each considered beam energy. The fits corresponds to values of  $\beta_r = 0.25$  and  $\beta_r = 0.35$ , respectively. Obviously, the distributions are consistent with a thermal freeze-out scenario as assumed in the blast model. This is also the case for the other investigated projectile–target combinations.

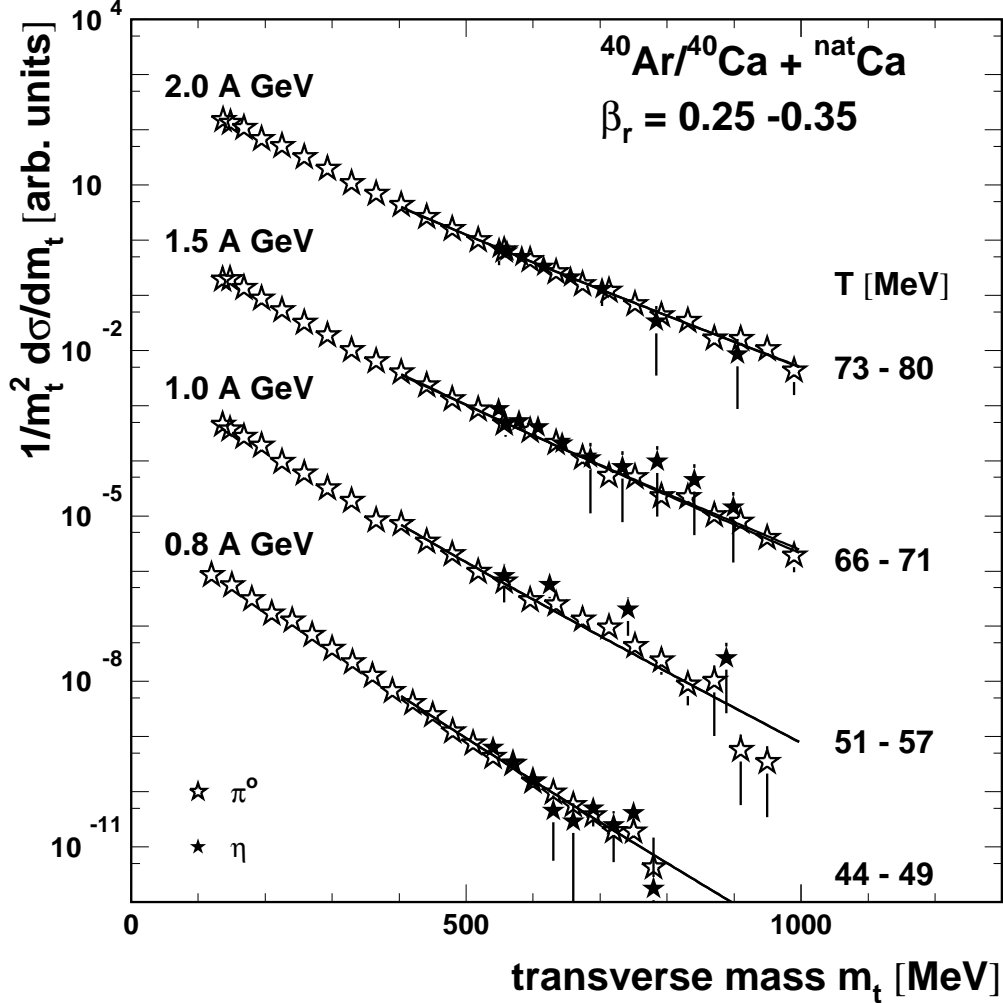


Fig. 7. Transverse-mass spectra of  $\pi^0$  and  $\eta$  mesons measured in the system  $^{40}\text{Ar}/^{40}\text{Ca} + ^{\text{nat}}\text{Ca}$  [20,21,26,28] at beam energies of 0.8, 1.0, 1.5, and 2.0 A GeV. The cross sections are scaled in arbitrary units. For each beam energy two lines are drawn which represent fits to the  $\pi^0$  data above transverse masses of 400 MeV using Eq. 12 with fixed transverse-expansion velocities of  $\beta_r = 0.25$  and  $0.35$ , respectively. On the scale chosen a difference between the two fits is not visible.

Fig. 8 shows the thermal freeze-out temperatures, again averaged over system size, as a function of the incident energy, together with the chemical freeze-out temperatures as obtained in the previous chapter. In addition, temperatures obtained in a blast-model analysis of  $\pi^-$ , proton, and deuteron spectra from the FOPI collaboration [12] are shown for comparison. With increasing beam energy the thermal as well as the chemical freeze-out temperatures grow. Within the error bars, chemical and thermal freeze-out temperatures overlap and agree nicely with the FOPI results. Our analysis, however, shows some trend towards lower temperatures at thermal freeze-out which one could expect since thermal freeze-out should not occur before chemical freeze-out.

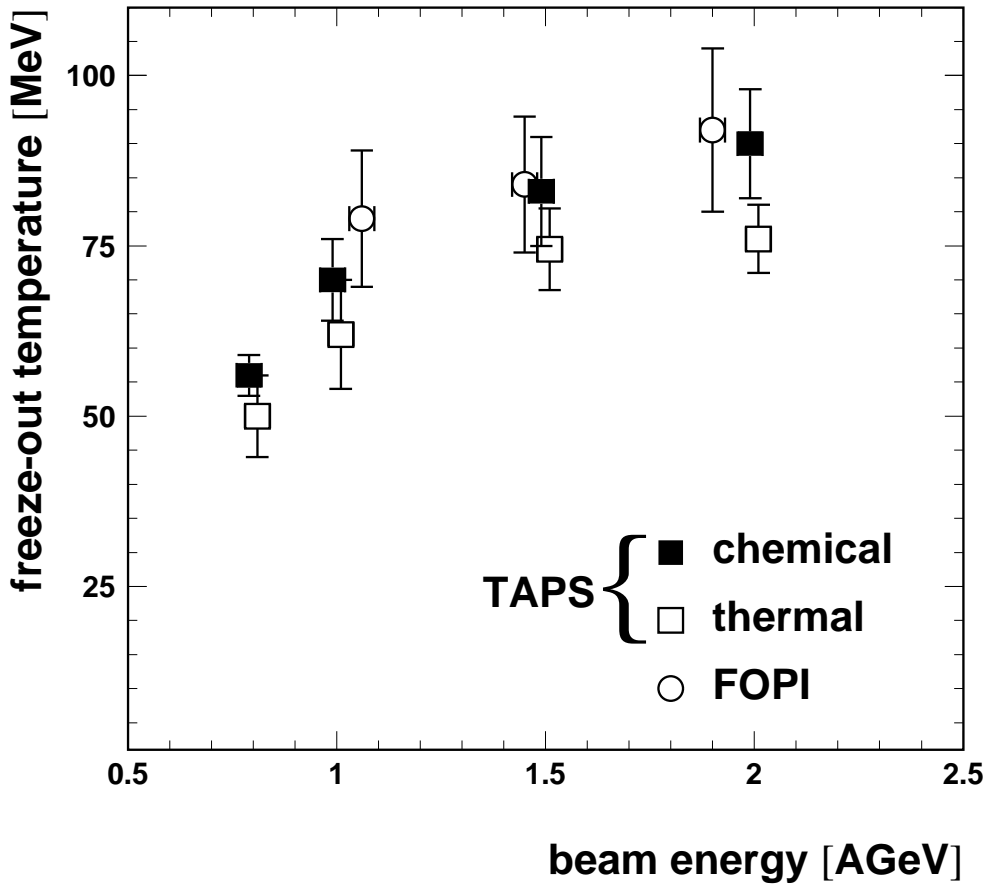


Fig. 8. System-size averaged thermal and chemical freeze-out temperatures, respectively, as function of the beam energy. Thermal freeze-out temperatures taken from [12] are shown for comparison.

Finally, we want to include our results on thermal freeze-out parameters into the phase diagram of hadronic matter as shown in Fig 5. To this aim one has to estimate the baryon chemical potential  $\mu_B$  at the moment of thermal freeze-out. If one assumes an isentropic expansion of the collision zone one can make use of the fact that the ratio  $T/\mu_B$  remains constant in that case. The baryon chemical potential at thermal freeze-out may then be calculated from the one at chemical freeze-out just by multiplication with the ratio of the temperatures. The resulting thermal freeze-out parameters are included in Fig. 5 together with a curve representing the thermal freeze-out of hadronic matter. While at SIS energies thermal and chemical freeze-out seem to almost coincide, at higher energies the freeze-out parameters clearly indicate that thermal freeze-out reflects a later stage of the collision process as lower temperatures compared to chemical freeze-out are deduced.

## 5 Conclusion

Neutral-pion and  $\eta$ -meson data measured near midrapidity in the energy range from 0.8A GeV to 2.0A GeV are consistent with the assumption that the hadronic fireball, which evolves during relativistic nucleus-nucleus collisions, may be in hadrochemical or thermal equilibrium at the moment of chemical or thermal freeze-out, respectively.

In contrast to ultrarelativistic collisions studied at AGS and SPS, chemical and thermal freeze-out seem to occur at almost the same stage of the expansion process at SIS energies. Another difference is that the freeze-out parameters at SIS are far below the phase boundary between a hadron gas and a quark-gluon plasma. This implies that the early stage of an ultrarelativistic nucleus-nucleus collision may come close to that phase transition while at SIS the early, high-density phase is described best by the term resonance matter.

Neutral-meson yields and spectra reflect only one facet of the very complex process of a relativistic nucleus-nucleus collision. With these observable alone it is not possible to decide whether chemical or thermal equilibrium, respectively, is actually reached during any stage of such a collision. Further experiments and analyses investigating complementary probes are necessary to clarify to what extent nucleus-nucleus collisions in the SIS-energy range can be described within the framework of equilibrium models.

## Acknowledgement

It is a pleasure to gratefully acknowledge helpful discussions with many colleagues, in particular, P. Braun-Munzinger, J. Cleymans, P. Danielewicz, R. Holzmann, V. Metag, P. Senger and R.S. Simon.

## References

- [1] R. Stock: Phys. Rep. 135 (1986) 259 and references therein
- [2] W. Cassing et al.: Phys. Rep. 188 (1990) 363
- [3] J. Aichelin: Phys. Rep. 202 (1991) 233
- [4] T. Maruyama et al.: Nucl. Phys. A 573 (1994) 653
- [5] S.A. Bass et al.: Phys. Rev. C 51 (1995) 3343
- [6] W. Ehehalt et al.: Phys. Rev. C 47 (1993) 2467

- [7] V. Metag: Prog. Part. Nucl. Phys. 30 (1993) 75
- [8] U. Mosel, V. Metag: Phys. Bl. 49 (1993) 426
- [9] S.H. Kahana et al.: Ann. Rev. Nucl. Part. Sci. 46 (1996) 31
- [10] M.C. Abreu et al.: Nucl. Phys. A 610 (1996) 404c
- [11] W. Reisdorf et al.: Nucl. Phys. A 612 (1997) 493
- [12] B. Hong et al.: Phys. Rev. C 57 (1998) 244
- [13] J. Cleymans and H. Satz: Z. Phys. C 57 (1993) 135
- [14] P. Braun-Munzinger et al.: Phys. Lett. B 344 (1995) 43
- [15] P. Braun-Munzinger et al.: Phys. Lett. B 365 (1996) 1
- [16] J. Sollfrank: J. Phys. G 23 (1997) 1903
- [17] B. Hong: in Proceedings of "Heavy Ion Physics at Low, Intermediate and Relativistic Energies using  $4\pi$  Detectors", Poiana Brasov, Romania, (1996) 304
- [18] J. Cleymans et al.: nucl-th/9711066
- [19] M. Pfeiffer: PhD thesis, University Gießen, 1993, unpublished
- [20] F.-D. Berg et al.: Phys. Rev. Lett. 72 (1994) 977
- [21] O. Schwalb et al.: Phys. Lett. B 321 (1994) 20
- [22] V. Metag: private communication
- [23] A. Schubert et al.: Nucl. Phys. A 583 (1995) 385 and private communication
- [24] M. Appenheimer: PhD thesis, University Gießen, 1997, unpublished
- [25] R. Auerbeck et al.: Z. Phys. A 359 (1997) 65
- [26] A. Marín et al.: Phys. Lett. B 409 (1997) 77
- [27] G. Martínez et al.: to be published
- [28] P. Vogt: PhD thesis, University Groningen, 1998, unpublished
- [29] A.R. Wolf et al.: submitted to Phys. Rev. Lett.
- [30] C. Müntz et al.: Z. Phys. A 357 (1997)
- [31] D. Pelte et al.: Z. Phys. A 357 (1997) 215
- [32] L. Simić: Phys. Rev. D 34 (1986) 692
- [33] J. Stachel, G.R. Young: Ann. Rev. Nucl. Part. Sc. 42 (1992) 537
- [34] M. Bourquin, J.M Gaillard: Nucl. Phys. B 114 (1976) 334
- [35] M. Aguilar-Benitez et al.: Z. Phys. C 50 (1991) 405

- [36] S.A. Bass et al.: Phys. Rev. Lett. 71 (1993) 1144
- [37] S. Teis et al.: Z. Phys. A 356 (1997) 421
- [38] R. Balian and C. Bloch: Ann. Phys. 70 (1970) 401
- [39] H.R. Jaqama et al.: Phys. Rev. C 29 (1984) 2067
- [40] R.M. Barnett et al.: Phys. Rev. D 54 (1996) 1
- [41] J.H. Koch et al.: Ann. Phys. 154 (1984) 99
- [42] R. Stock: Nucl. Phys. A 630 (1998)
- [43] H. Weber: Diploma thesis, University Frankfurt, 1996, unpublished
- [44] P.J. Siemens and J.O. Rasmussen: Phys. Rev. Lett. 42 (1979) 880
- [45] N. Herrmann: Nucl. Phys. A 610 (1996) 49c